Ab Initio Insights into Charge Localization in Bismuth Oxyhalides BiOX (X = F, Cl, Br, I)

THE JOURNAL OF PHYSICAL CHEMISTRY C
A JOURNAL OF THE AMERICAN CHEMICAL SOCIETY

pubs.acs.org/JPCC

Article

Ab Initio Insights into Charge Localization in Bismuth Oxyhalides BiOX (X = F, Cl, Br, I)

Hassan Ouhbi and Julia Wiktor*

Cite This: *J. Phys. Chem. C* 2022, 126, 19956−19961

Read Online

ACCESS | Metrics & More | Article Recommendations

ABSTRACT: Developing efficient photocatalysts for clean energy generation is crucial to achieving net-zero emissions. To this end, we investigate the behavior of photoexcited charges in bismuth oxyhalides BiOX (X = F, Cl, Br, and I), a family of inexpensive and promising photocatalysts. To model the localization of excess electrons and holes, we use hybrid density functional theory PBE0(α). Our results indicate that electron polarons are unstable in these materials. Concurrently, we find that hole localization is favorable, and we identify two different possible configurations in which polarons are formed. One consists of two dimerized halogen atoms (V_K center) and is preferentially formed in BiOBr and BiOI with binding energies that amount to −0.26 and −0.21 eV, respectively. The other corresponds to localization on a single Bi site and the surrounding oxygen and halogen atoms (Bi_{XO}). This form of polaron is favorable in BiOF and BiOCl with binding energies that amount to −0.35 and −0.23 eV, respectively. These findings highlight the behavior of photogenerated carriers and may open up avenues for future investigations on carrier transport in bismuth oxyhalides.

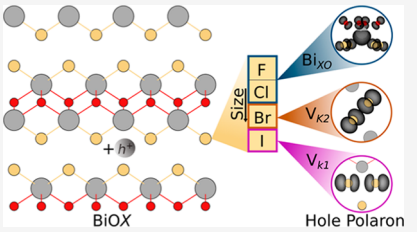

INTRODUCTION

Semiconductor photocatalysts are widely applied in solar-to-chemical conversion: CO_2 reduction reaction,[1] water splitting, or N_2 fixation to ammonia.[2] The concept here is to mimic plants' photosynthesis, where the semiconductor will be used to harvest solar radiation. In the past decade, bismuth oxyhalides with the formula BiOX (X = F, Cl, Br, and I) have emerged as potential photocatalysts owing to their nontoxicity, structural flexibility (accommodation of different halogens), and low cost.[3−6] All BiOX compounds crystallize in the tetragonal Matlockite structure (see Figure 1), which represents the simplest form of Sillén-type structures with the general formula $[M_2O_2][X_m]$.[7] Moreover, they exhibit a layered structure comprising repeated [X−Bi−O−X] slabs which are connected by van der Waals interactions, and each bismuth atom is eight-coordinated *via* strong covalent bonding by four halogens (X) and four oxygens.[8]

As for their electronic structure, the conduction band is dominated by Bi 6p states in all BiOX compounds. Additionally, their valence band is mainly composed of X *n*p (*n* = 2, 3, 4, 5 for F, Cl, Br, and I, respectively) states and O 2p states. Generally, the halogens *n*p orbitals are located at higher energies than O 2p ones, except for X = F due to its higher electronegativity.[9] Varying the halogen size was found to cause an upward shift of valence band maximum (VBM), in accordance with the reduced electronegativity from F to I, and a downward shift of the Bi-dominated conduction band minimum.[9−11] Consequently, the band gaps of BiOX compounds decrease from 4.01 for BiOF to 1.85 eV for BiOI (see Table 1). Hence, the light absorption is extended from the ultraviolet (for BiOF and BiOCl)[12] to the visible region (for BiOBr and BiOI).[13]

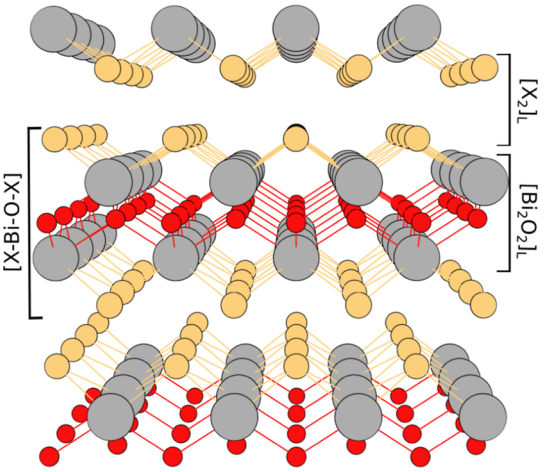

Figure 1. Crystal structure of BiOX systems with a Sillén-type structure and *P*4/*nmm* space group. The elements Bi, X, and O are shown in gray, yellow, and red, respectively.

Besides high photoabsorption, the layered bismuth oxyhalides exhibit an extraordinary capability of separating and transferring the charges due to an internal electric field perpendicular to

Received: September 21, 2022
Revised: October 26, 2022
Published: November 9, 2022

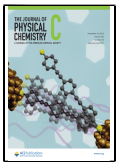

Table 1. Experimental Lattice Parameters and Band Gaps of the Considered Oxyhalides (from Refs 10 and 11)[a]

material	a (Å)	c (Å)	α	E_{gap}^{exp}(eV)
BiOF	3.76	6.23	0.26	4.01
BiOCl	3.89	7.37	0.24	3.44
BiOBr	3.92	8.10	0.23	2.76
BiOI	4.00	9.14	0.24	1.85

[a] α is the fraction of Fock exchange used in the PBE0(α) functional, as derived based on Koopmans' condition.

$[Bi_2O_2]$ and $[X_2]$ layers.[12,13] We will refer to these layers by $[Bi_2O_2]_L$ and $[X_2]_L$, respectively (see Figure 1). Therefore, the photogenerated charges have more chances to diffuse through the materials and thus reach the surface where the reactions take place. Although many works have reported the importance of this internal feature, the behavior of the excess charges has not been investigated in detail, especially in the presence of lattice distortions that can cause charge self-trapping through the formation of polarons. Meanwhile, electron and hole localizations have been observed in metal oxides and alkali halides and, therefore, can also be expected in the family of oxyhalides. Due to the structural complexity of these materials, there are multiple configurations in which charges can potentially localize. For instance, in alkali halides,[14] polarons are found to localize on pairs of halogen atoms, forming a bond between them and leading to their dimerization. This corresponds to the formation of so-called V_K centers.[15] In perovskites,[16,17] charges are often found to localize around a single atom like in $SrTiO_3$ (Ti site for the electron and O site for the hole),[18,19] $NaTaO_3$ (O site for the hole),[20] or $CsPbBr_3$ (Pb site for the electron).[21] Another possibility is a multisite localization like in the case of $BiOV_4$ where a hole is trapped at a Bi site with eight oxygens around it.[22] Given that BiOX materials possess two distinct compositions (halide in $[X_2]_L$ and oxide in $[Bi_2O_2]_L$), it is, therefore, of high interest to investigate the stability of all aforementioned polaronic states.

In this work, we study the behavior of the photogenerated holes and electrons in bismuth oxyhalides BiOX (X = F, Cl, Br, and I) by using hybrid functional PBE0(α),[23] where α values fulfill Koopmans' condition[24] (see Table 1). We investigate different structural distortions associated with polaron formation and show that hole trapping in V_K centers is only favorable in BiOI and BiOBr. Hole trapping in BiOCl and BiOF, on the other hand, is predicted to occur in a multisite configuration where the hole is localized on a Bi site and the surrounding oxygen and halogen atoms. At variance, we have found that electron polarons are not stable in any of the considered bismuth oxyhalides.

METHODS

In this study, we performed first-principles calculations in the framework of hybrid functional PBE0(α)[23] with D3 van der Waals (vdW) interactions by Grimme[25] as implemented in the CP2K package.[26] For each compound, we apply Koopmans' theorem to find the α parameter. We focus on the vertical (+2/+1) transition of an unrelaxed oxygen vacancy, following the same procedure as in ref 20 To compute the finite-size corrections needed to identify the single-particle energy levels, we adopt the approach by Falletta *et al.*[27] In the correction scheme, we use the reported theoretical values of the high-frequency dielectric constant from ref 28. The obtained α values are listed in Table 1. Furthermore, we employ Gaussian-type DZVP-MOLOPT basis sets[29] with a cutoff energy of 650 Ry to expand the electron density into plane waves. To describe the core−valence interactions, Goedecker−Teter−Hutter pseudopotentials are used.[30] To improve the performance of Hartree−Fock exchange calculations, we use cFIT-type auxiliary density matrix method[31] basis sets for all elements. We consider a 4 × 4 × 2 tetragonal Matlockite supercell of bismuth oxyhalides BiOX (X = F, Cl, Br, and I) containing 192 atoms, with experimental lattice parameters as summarized in Table 1. We note that in the present computational setup, the spin−orbit coupling (SOC) is not taken into account. However, we expect that in the case of hole polarons, their stability can be at most reduced by the increase of the VBM due to SOC,[21,32] which has been found to be only significant in BiOI and amount to 0.11 eV.[9]

RESULTS AND DISCUSSION

We begin by assessing the stability of electron polarons in the BiOX materials. Because the Bi 6p states dominate their conduction band, we add an electron to supercells with various starting structural distortions around the Bi site, corresponding to elongating one or several Bi−X and Bi−O bonds. The electron delocalizes during the geometry optimization of all considered structures, thus suggesting that electron polarons are not stable in bismuth oxyhalides.

We now focus on hole polarons in BiOX compounds. In all bismuth oxyhalides, the valence band is composed of a mixture of O 2p states and X *n*p states, and the contribution of the latter increases as the ionic radius increases (from F to I). Considering this, we expect that the nature of hole polarons can vary from oxygen- to halogen-related localization. We therefore explore the possible localization modes both within $[Bi_2O_2]_L$ and $[X_2]_L$ (see Figure 1). First, we investigate the possibility of a single-site self-trapping either on the oxygen atom in the $[Bi_2O_2]_L$ layer or on the halogen atom in the $[X_2]_L$ layer. We apply multiple structural distortions by elongating the Bi−O bonds (for oxygen site localization) or the Bi−X bonds (for halogen site localization), and we introduce a hole into the system. However, following geometry optimization, we find that the hole is delocalized, with spin density distributed over all O and X sites in all BiOX materials, indicating that this type of localization is unstable.

To assess the stability of the so-called V_K center (X_2 dimers), we displace the first-nearest-neighbors X ion pairs toward each other to form initial polaron seed structures. After geometry relaxation, we observe hole localization in all considered materials except for BiOF, as can be seen from the spin densities illustrated in Figure 2. We note that in BiOCl, BiOBr, and BiOI, we find two different forms of X_2 dimers, one involving halogen atoms from the same layer, called V_{K1}, and one involving halogen atoms from two parallel atomic layers, called V_{K2} (see Figure 2). We now analyze the projected densities of state (PDOS) corresponding to the V_K center in each of the materials (see right panels in Figure 3) to verify which atoms contribute to the polaronic state. The PDOS shows that the hole polaron state primarily consists of X *n*p orbitals, and it appears above the VBM at an energy level of 1.6, 1.4, and 0.9 eV for BiOCl, BiOBr, and BiOI, respectively. We note that the absence of the V_K centers in BiOF can be rationalized based on the fact that in this material, in contrast to other oxyhalides, the highest occupied halogen states are found below the oxygen-related ones.

The V_K center formation is accompanied by an inward displacement of the halogen atoms forming the dimer, which leads to the shortening of the X−X distance. Figure 2 shows the

https://doi.org/10.1021/acs.jpcc.2c06711
J. Phys. Chem. C 2022, 126, 19956−19961

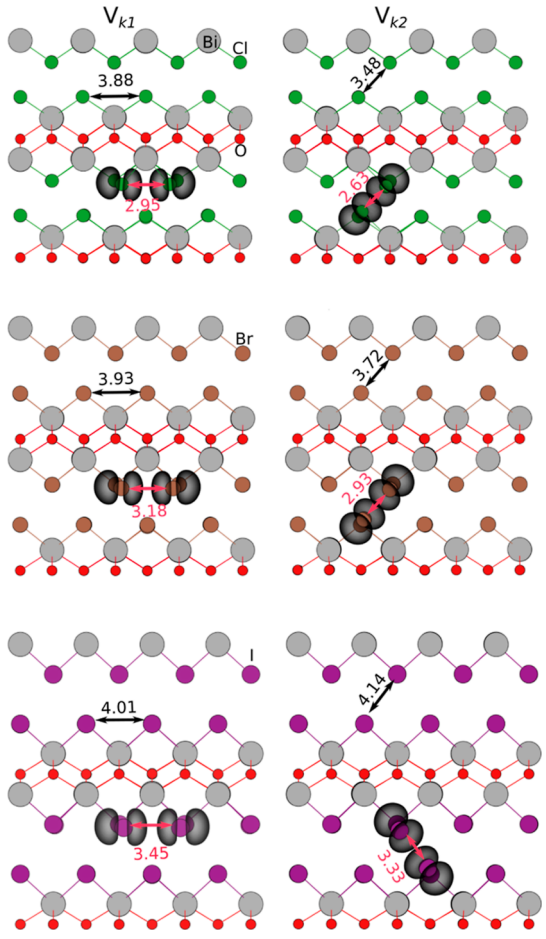

Figure 2. Localized state with the hole trapped on dimers formed by intralayer (V_{K1}) and interlayer halogens X (V_{K2}). The isosurface value is 0.045 e/Å^3.

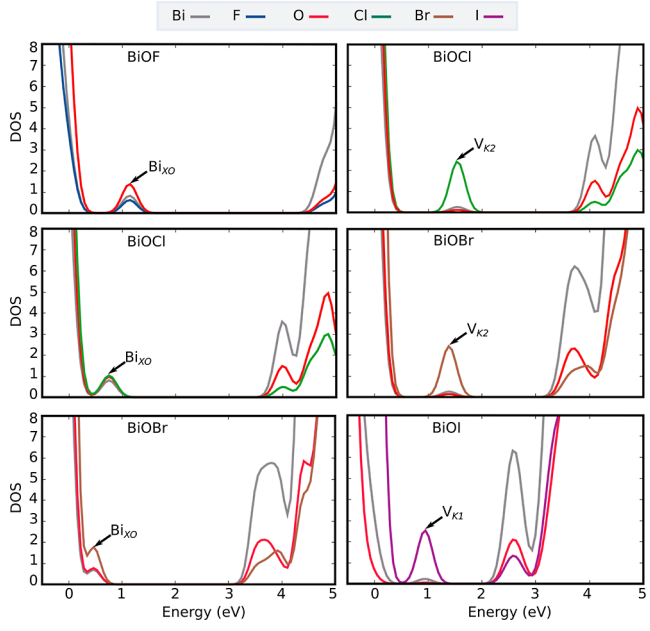

Figure 3. PDOS of the hole-trapped states in the Bi_{XO} (left panels) and V_K center (right panels) configurations.

two possible dimer configurations in BiOCl, BiOBr, and BiOI. In particular, in BiOCl, the Cl−Cl distance amounts to 2.95 Å in the V_{K1} center, compared to the equilibrium Cl−Cl distance of 3.88 Å in the pristine material. The distance is smaller in the V_{K2} configuration (2.63 Å), consistent with the smaller equilibrium distance in the neutral system (3.48 Å). Similar trends can be found in BiOBr and BiOI, where the X−X is also longer in the V_{K1} center (3.18 and 3.45 Å, respectively) than in the V_{K2} center (2.93 and 3.33 Å, respectively). We remark that the calculated X−X distances are comparable with those reported for V_K centers in CH_3NH_3PbX (X = Cl, Br, I) in a previous theoretical study.[33]

We note that while neither of the V_K center configurations is stable in BiOF, the geometrical optimizations starting from various initial distortions lead instead to a state where the hole is localized on a Bi site and the surrounding halogen and oxygen atoms (Bi_{XO} localization). To investigate the structural distortion driving the system to localize the hole in this configuration, we analyze the geometry of this polaronic state. In Figure 4, we show that the lattice distortion associated with Bi_{XO}

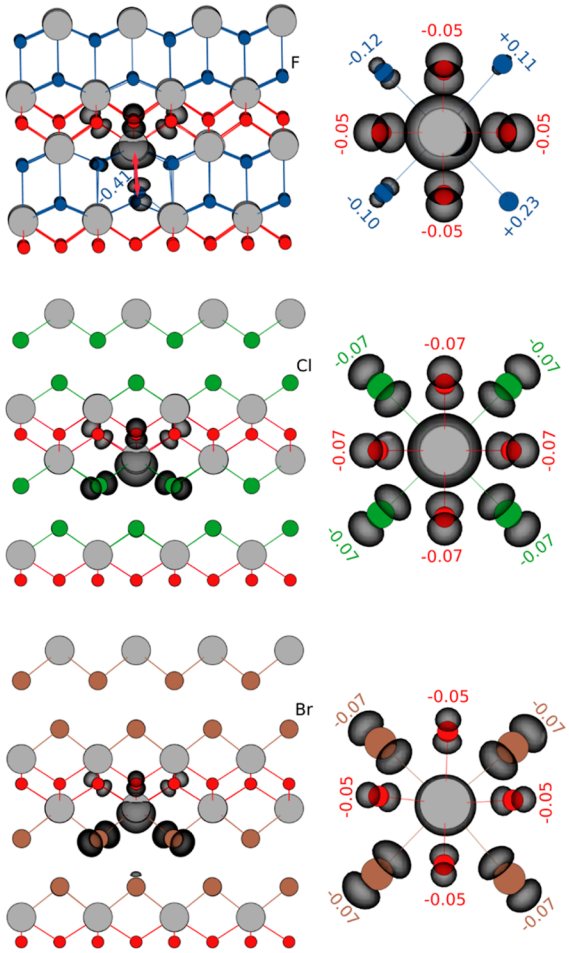

Figure 4. Bi_{XO} configuration of a hole localized on a Bi site and the surrounding X and O sites. The iso-surface value is 0.045 e/Å^3.

configuration in BiOF is mainly related to a substantial upward displacement of a fluorine atom located in the [X−Bi−O−X] slab beneath, resulting in the shortening of the Bi−F distance by 0.41 Å. The other Bi−F bonds are also affected, with two of them becoming shorter and two others longer than in the pristine structure (see Figure 4).

While the Bi_{XO} configuration is spontaneously formed only in BiOF, it can still correspond to at least a local minimum in other

https://doi.org/10.1021/acs.jpcc.2c06711
J. Phys. Chem. C 2022, 126, 19956−19961

oxyhalides. Therefore, we also initialize such a state in BiOCl, BiOBr, and BiOI. After geometry relaxation, the hole remains localized in this configuration in both BiOCl and BiOBr. In these compounds, we however observe a more symmetrical contraction of Bi−O (on average −0.06 Å) and Bi−X bond length (−0.07 Å), and the absence of any halogen displacement located underneath [X−Bi−O−X] slab of both BiOCl and BiOBr (see Figure 4). To further assess the participation of different states in the Bi_{XO} polaron, we consider the corresponding PDOS, as given in Figure 3. In all compounds exhibiting this type of hole localization, the composition of the localized state is in accordance with the spin density distribution shown in Figure 4. The contribution of Bi 6s remains almost constant in the three compounds. At the same time, the O 2p contribution decreases gradually when the halogen atom changes in the F−Cl−Br order and that of X *n*p increases. At variance, this type of distortion turned out to be unstable in BiOI, where the structure returned to its pristine state after the relaxation and hole delocalization, meaning that in BiOI, holes only localize in V_K centers. We can generalize that halogens with larger atomic radius localization in the V_K center are more likely, while for smaller halogen atoms, the Bi_{XO} configuration can be expected. Therefore, we conclude that there is a correlation between halogen size and the possible modes of hole localizations.

To understand the effect of varying the halogen atom in the BiOX compound on the stability of the polaronic configurations, we calculate their binding energies as follows

$$E_b = E_{+1}[\text{polaron}] - E_0[\text{pristine}] + q\epsilon_v + E_{corr}$$

where E_0 [pristine] is the energy of the neutral nondistorted structure, E_{+1} is the energy of the fully relaxed polaron state, with $q = +1$ denoting the excess of charge of a hole, ϵ_v is the position of the VBM, and E_{corr} is the electrostatic finite-size correction, calculated according to the scheme proposed by Freysoldt, Neugebauer, and Van de Walle (FNV).[34] We note that the negative binding energy of a polaronic state means that it is energetically favorable.

The obtained binding energies of hole polarons in various configurations are given in Table 2. By analyzing the binding energies of all polaronic states, we can generally conclude that the stability of the V_K center increases and the stability of Bi_{XO} decreases when the halogen atom becomes larger. The only exceptions from this trend are the binding energies of V_{K2} in BiOBr and BiOI. To further understand the trends across the considered materials, we decompose the polaron binding energies into the electronic energy gain due to the hole localization E_{el} and the structural deformation cost E_{st}. E_{el} is calculated as the vertical energy difference between the delocalized and localized states in the polaronic configuration (see Figure 5). The deformation cost is calculated as the difference in total energies of the neutral pristine and distorted system, with $E_{st} = E_{distorted} - E_{pristine}$. The variation of these two quantities as a function of the halogen size is given in Figure 5. We note that for each of the quantities E_b, E_{st}, and E_{el}, we apply appropriate finite-size corrections.[27,34]

Table 2. Calculated Binding Energies of Hole Polarons in Different Configurations

	E_b (hole) (eV)		
	V_{K1}	V_{K2}	Bi_{XO}
BiOF	unstable	unstable	−0.35
BiOCl	+0.39	−0.08	−0.23
BiOBr	−0.01	−0.26	−0.15
BiOI	−0.23	−0.21	unstable

We first analyze the stability trends for the V_K centers in the considered materials. As mentioned previously, hole localization in the form of the V_K center is not stable in BiOF. This stems from the fact that fluorine has a higher electronegativity than oxygen, which causes the VBM to be composed of more oxygen 2p states than fluorine 2p.[9] As shown in Figure 5, the individual energy contributions of E_{st} and E_{el} correlate with the size of the halogen. The trend is the clearest for the structural deformation cost, which is the highest in BiOCl and the lowest in BiOI. The electronic energy gain due to localization has a less clear trend, but generally, this gain increases when the size of the halogen atom decreases. The binding energies of the V_K centers being the sum of these contributions ($E_b = E_{st} + E_{el}$) also do not follow the size of the halogen in a straightforward way. Focusing on the binding energies of the V_{K2} center, we note that this defect is the most stable in BiOBr (E_b of −0.26 eV), followed by BiOI (E_b of −0.21 eV) and BiOCl (E_b of −0.08 eV). The fact that the V_{K2} center is more stable in BiOBr than in BiOI is mainly related to the relatively low value of the electronic energy gain E_{el} in the iodide. The binding energy of the V_{K1} center is only negative in BiOBr and BiOI, which can be explained by the weaker electronic energy gain found in this state. In BiOBr, the stability of V_{K1} is very low (E_b of −0.01 eV), while it is the most favorable configuration for hole localization in BiOI with an E_b of −0.23 eV.

We now analyze the stability trends of the Bi_{XO} configuration. In BiOF, it is the only stable form of hole localization and also the most polaronic state in the BiOX family overall (E_b of −0.35 eV) owing to its high electronic energy gain compared to the cases of BiOCl and BiOBr. In BiOCl, this configuration is also the most favorable polaronic state, with a binding energy of −0.23 eV (as compared to −0.08 eV for the more stable V_{K2} center). We note that despite the high electronic energy gain of V_{K2} compared to Bi_{XO}, the low structural deformation cost E_{st} leads to the highest stability of Bi_{XO} in BiOCl. In BiOBr, the Bi_{XO} configuration is still stable (binding energy of −0.15 eV), but less stable than V_{K2} because of the significantly lower electronic energy gain. In BiOI, we find the Bi_{XO} configuration to be unstable. Overall, the stability of Bi_{XO} polaronic decreases in accordance with the reduced electronegativity (from F to I).

Our findings on hole localization in BiOX compounds can be related to expected charge mobilities in these materials. Considering that we find at least one stable form of hole polarons in each oxyhalide, we can expect that hole diffusion proceeds *via* a hopping mechanism with suppressed mobilities. It is worth noting that there are various models to evaluate the mobility of charge carriers, such as the Marcus−Emin−Holstein−Austin−Mott model.[35,36] Their application is, however, beyond the scope of this study. Nevertheless, we can suggest speculative scenarios of hole migration in BiOX materials based on different hole localization modes. We propose that in BiOF and BiOCl, where the hole is favorably localized in the Bi_{XO} configuration, the in-plane migration of the hole might occur through smooth hopping transfer across Bi sites in the $[Bi_2O_2]_L$ layers. However, in the *z* direction, the hole mobility would be further reduced. In BiOF, the hole would have to migrate from one Bi site to another through a delocalized transition state due to the lack of any localization mode at the $[X_2]_L$ layer. In the case of BiOCl, the hole would have to be

https://doi.org/10.1021/acs.jpcc.2c06711
J. Phys. Chem. C 2022, 126, 19956−19961

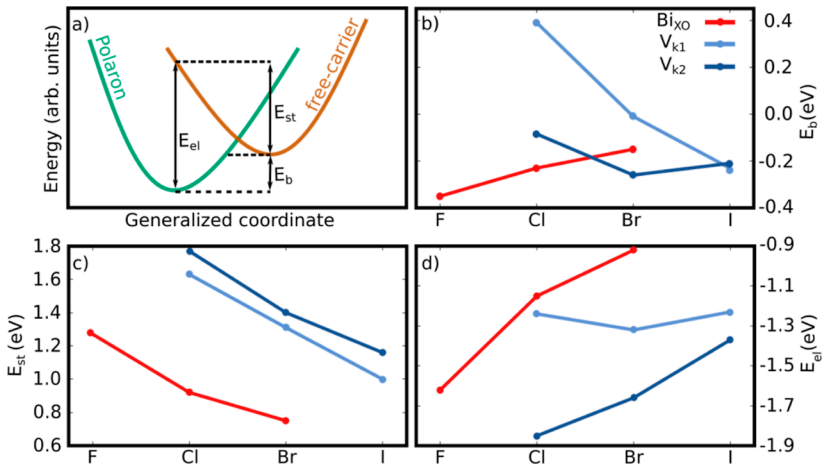

Figure 5. (a) Sketch of the configuration coordinate diagram showing the polaronic energy (E_b), structural energy cost (E_{st}), and electronic energy gain (E_{el}) energies as a function of lattice distortion for the polaronic and delocalized configuration. (b–d) Variation of E_b, E_{st}, and E_{el} as a function of halogen type.

transferred *via* the V_{K2} polaronic transition state. In BiOBr and BiOI, the in-plane hole diffusion would most likely happen through a charge transfer between the V_K centers. In the *z* direction, the hole would have to move from one V_K center to another *via* Bi_{XO} configuration for BiOBr and a delocalized state in the case of BiOI (because of the instability of Bi_{XO} configuration).

While small mobilities are expected for excess holes in the considered materials, we have not found any form of electron localization, suggesting that these charges remain delocalized and can quickly migrate *via* a band-like process to the surface. This expected difference in the mobility of the electrons and the holes could either positively affect the performance of bismuth oxyhalide photocatalysts (by reducing electron–hole recombination rate) or negatively by reducing their activity (because of the slow hole diffusion) and would be interesting to study in the future.

Conclusions. In this work, we studied the behavior of the photogenerated holes and electrons in bismuth oxyhalides. We first demonstrated that the electron polaron formation is generally not favorable in BiOX oxyhalides. However, hole polaron localization is predicted to be favorable and exhibits different configurations depending on the halogen type. In particular, our analysis reveals that in BiOF and BiOCl, holes preferentially localize on a single bismuth site and the surrounding oxygen and halogen atoms. On the other hand, in BiOBr and BiOI, the hole preferentially localizes in the form of a V_K center. We demonstrated that the compositions of the valence band and atomic radius are major factors defining the nature of the polaron configuration. Our findings suggest that electrons in these materials are most likely propagating *via* a band-like mechanism, whereas holes diffuse by polaronic hopping between favorable configurations. Furthermore, we discussed the implications of these results for applications of bismuth oxyhalides in photocatalysis. Finally, we believe these insights into the behavior of the photogenerated carriers in the BiOX series offer guidelines for future studies.

AUTHOR INFORMATION

Corresponding Author

Julia Wiktor – *Department of Physics, Chalmers University of Technology, SE-412 96 Gothenburg, Sweden;* orcid.org/0000-0003-3395-1104; Email: julia.wiktor@chalmers.se

Author

Hassan Ouhbi – *Department of Physics, Chalmers University of Technology, SE-412 96 Gothenburg, Sweden;* orcid.org/0000-0001-7371-4782

Complete contact information is available at: https://pubs.acs.org/10.1021/acs.jpcc.2c06711

Notes

The authors declare no competing financial interest.

ACKNOWLEDGMENTS

The authors acknowledge funding from the "Area of Advance—Materials Science" at the Chalmers University of Technology and the Swedish Research Council (2019-03993). The computations were performed on resources provided by the Swedish National Infrastructure for Computing (SNIC) at the NSC, C3SE, and PDC. This work was supported by the Chalmers Gender Initiative for Excellence (Genie).

REFERENCES

(1) Shi, Y.; Li, J.; Mao, C.; Liu, S.; Wang, X.; Liu, X.; Zhao, S.; Liu, X.; Huang, Y.; Zhang, L. Van Der Waals gap-rich BiOCl atomic layers realizing efficient, pure-water CO2-to-CO photocatalysis. *Nat. Commun.* **2021**, *12*, 5923.

(2) Li, H.; Shang, J.; Shi, J.; Zhao, K.; Zhang, L. Facet-dependent solar ammonia synthesis of BiOCl nanosheets via a proton-assisted electron transfer pathway. *Nanoscale* **2016**, *8*, 1986–1993.

(3) Li, H.; Shang, J.; Zhu, H.; Yang, Z.; Ai, Z.; Zhang, L. Oxygen vacancy structure associated photocatalytic water oxidation of BiOCl. *ACS Catal.* **2016**, *6*, 8276–8285.

(4) Li, H.; Shang, J.; Ai, Z.; Zhang, L. Efficient Visible Light Nitrogen Fixation with BiOBr Nanosheets of Oxygen Vacancies on the Exposed {001} Facets. *J. Am. Chem. Soc.* **2015**, *137*, 6393–6399.

(5) Guan, M.; Xiao, C.; Zhang, J.; Fan, S.; An, R.; Cheng, Q.; Xie, J.; Zhou, M.; Ye, B.; Xie, Y. Vacancy associates promoting solar-driven photocatalytic activity of ultrathin bismuth oxychloride nanosheets. *J. Am. Chem. Soc.* **2013**, *135*, 10411–10417.

(6) Wang, W.; Huang, F.; Lin, X. xBiOI-(1−x)BiOCl as efficient visible-light-driven photocatalysts. *Scr. Mater.* **2007**, *56*, 669−672.
(7) Bannister, F. A. The crystal-structure of the bismuth oxyhalides. *Mineral. Mag.* **1935**, *24*, 49−58.
(8) Keller, E.; Krämer, V. A Strong Deviation from Vegard's Rule: X-Ray Powder Investigations of the Three Quasi-Binary Phase Systems BiOX-BiOY (X, Y = Cl, Br, I). *Z. Naturforsch. B* **2005**, *60*, 1255−1263.
(9) Ganose, A. M.; Cuff, M.; Butler, K. T.; Walsh, A.; Scanlon, D. O. Interplay of orbital and relativistic effects in bismuth oxyhalides: BiOF, BiOCl, BiOBr, and BiOI. *Chem. Mater.* **2016**, *28*, 1980−1984.
(10) Kan, Y.; Teng, F.; Yang, Y.; Xu, J.; Yang, L. Direct conversion mechanism from BiOCl nanosheets to BiOF, Bi7F11O5 and BiF3 in the presence of a fluorine resource. *RSC Adv.* **2016**, *6*, 63347−63357.
(11) An, H.; Du, Y.; Wang, T.; Wang, C.; Hao, W.; Zhang, J. Photocatalytic properties of BiOX (X = Cl, Br, and I). *Rare Met.* **2008**, *27*, 243−250.
(12) Zhang, K.-L.; Liu, C.-M.; Huang, F.-Q.; Zheng, C.; Wang, W.-D. Study of the electronic structure and photocatalytic activity of the BiOCl photocatalyst. *Appl. Catal., B* **2006**, *68*, 125−129.
(13) Zhang, J.; Shi, F.; Lin, J.; Chen, D.; Gao, J.; Huang, Z.; Ding, X.; Tang, C. Self-assembled 3-D architectures of BiOBr as a visible light-driven photocatalyst. *Chem. Mater.* **2008**, *20*, 2937−2941.
(14) Sadigh, B.; Erhart, P.; Åberg, D. Variational polaron self-interaction-corrected total-energy functional for charge excitations in insulators. *Phys. Rev. B: Condens. Matter Mater. Phys.* **2015**, *92*, 075202.
(15) Känzig, W. Electron Spin Resonance ofV1-Centers. *Phys. Rev.* **1955**, *99*, 1890−1891.
(16) Yin, J.; Li, H.; Cortecchia, D.; Soci, C.; Brédas, J.-L. Excitonic and Polaronic Properties of 2D Hybrid Organic-Inorganic Perovskites. *ACS Energy Lett.* **2017**, *2*, 417−423.
(17) Peng, C.; Wang, J.; Wang, H.; Hu, P. Unique Trapped Dimer State of the Photogenerated Hole in Hybrid Orthorhombic CH3NH3PbI3 Perovskite: Identification, Origin, and Implications. *Nano Lett.* **2017**, *17*, 7724−7730.
(18) Hao, X.; Wang, Z.; Schmid, M.; Diebold, U.; Franchini, C. Coexistence of trapped and free excess electrons in $SrTiO_3$. *Phys. Rev. B: Condens. Matter Mater. Phys.* **2015**, *91*, 085204.
(19) Chen, H.; Umezawa, N. Hole localization, migration, and the formation of peroxide anion in perovskite $SrTiO_3$. *Phys. Rev. B: Condens. Matter Mater. Phys.* **2014**, *90*, 035202.
(20) Ouhbi, H.; Wiktor, J. Polaron formation and hopping in tantalate perovskite oxides: NaTaO3 and KTaO3. *Phys. Rev. B* **2021**, *104*, 235158.
(21) Österbacka, N.; Erhart, P.; Falletta, S.; Pasquarello, A.; Wiktor, J. Small Electron Polarons in CsPbBr3: Competition between Electron Localization and Delocalization. *Chem. Mater.* **2020**, *32*, 8393−8400.
(22) Wiktor, J.; Pasquarello, A. Electron and Hole Polarons at the BiVO4-Water Interface. *ACS Appl. Mater. Interfaces* **2019**, *11*, 18423−18426.
(23) Perdew, J. P.; Ernzerhof, M.; Burke, K. Rationale for mixing exact exchange with density functional approximations. *J. Chem. Phys.* **1996**, *105*, 9982−9985.
(24) Dabo, I.; Ferretti, A.; Poilvert, N.; Li, Y.; Marzari, N.; Cococcioni, M. Koopmans' condition for density-functional theory. *Phys. Rev. B: Condens. Matter Mater. Phys.* **2010**, *82*, 115121.
(25) Grimme, S.; Ehrlich, S.; Goerigk, L. Effect of the damping function in dispersion corrected density functional theory. *J. Comput. Chem.* **2011**, *32*, 1456−1465.
(26) VandeVondele, J.; Krack, M.; Mohamed, F.; Parrinello, M.; Chassaing, T.; Hutter, J. Quickstep: Fast and accurate density functional calculations using a mixed Gaussian and plane waves approach. *Comput. Phys. Commun.* **2005**, *167*, 103−128.
(27) Falletta, S.; Wiktor, J.; Pasquarello, A. Finite-size corrections of defect energy levels involving ionic polarization. *Phys. Rev. B* **2020**, *102*, 041115.
(28) Ran, Z.; Wang, X.; Li, Y.; Yang, D.; Zhao, X.-G.; Biswas, K.; Singh, D. J.; Zhang, L. Bismuth and antimony-based oxyhalides and chalcohalides as potential optoelectronic materials. *npj Comput. Mater.* **2018**, *4*, 14.
(29) VandeVondele, J.; Hutter, J. Gaussian basis sets for accurate calculations on molecular systems in gas and condensed phases. *J. Chem. Phys.* **2007**, *127*, 114105.
(30) Goedecker, S.; Teter, M.; Hutter, J. Separable dual-space Gaussian pseudopotentials. *Phys. Rev. B: Condens. Matter Mater. Phys.* **1996**, *54*, 1703−1710.
(31) Guidon, M.; Hutter, J.; VandeVondele, J. Auxiliary Density Matrix Methods for Hartree−Fock Exchange Calculations. *J. Chem. Theory Comput.* **2010**, *6*, 2348−2364.
(32) Ouhbi, H.; Ambrosio, F.; De Angelis, F.; Wiktor, J. Strong electron localization in tin halide perovskites. *J. Phys. Chem. Lett.* **2021**, *12*, 5339−5343.
(33) Whalley, L. D.; Crespo-Otero, R.; Walsh, A. H-center and V-center defects in hybrid halide perovskites. *ACS Energy Lett.* **2017**, *2*, 2713−2714.
(34) Freysoldt, C.; Neugebauer, J.; Van de Walle, C. G. Fully ab initio finite-size corrections for charged-defect supercell calculations. *Phys. Rev. Lett.* **2009**, *102*, 016402.
(35) Austin, I. G.; Mott, N. F. Polarons in crystalline and non-crystalline materials. *Adv. Phys.* **2001**, *50*, 757−812.
(36) Emin, D.; Holstein, T. Studies of small-polaron motion IV. Adiabatic theory of the Hall effect. *Ann. Phys.* **1969**, *53*, 439−520.

https://doi.org/10.1021/acs.jpcc.2c06711
J. Phys. Chem. C 2022, 126, 19956−19961